Journal of Zhejiang University-SCIENCE A (Applied Physics & Engineering)
ISSN 1673-565X (Print); ISSN 1862-1775 (Online)
www.jzus.zju.edu.cn; www.springerlink.com
E-mail: jzus@zju.edu.cn

Discrete element method-based prediction of areas prone to buried hill-controlled earth fissures*

Yang LIU[1,2], Dan ZHANG[†‡1,2], Guang-ya WANG[2], Chun LIU[1], Yan ZHANG[2]

[1]*School of Earth Sciences and Engineering, Nanjing University, Nanjing 210023, China*

[2]*Key Laboratory of Earth Fissures Geological Disaster of Ministry of Land and Resources, Geological Survey of Jiangsu Province, Nanjing 210018, China*

[†]E-mail: zhangdan@nju.edu.cn

Received June 27, 2019; Revision accepted Sept. 3, 2019; Crosschecked Sept. 10, 2019

Abstract: An independently developed discrete element code, MatDEM, was used to simulate buried hill-controlled earth fissures. An initial cubic discrete element method (DEM) model was obtained by considering the gravity accumulation of particles. A 2D stratigraphic model can be constructed by importing an elevation table of different strata into a cubic model. A simplified fluid-structure interaction method was then introduced to this. The model was simulated by gradually lowering the water level and then calculating the compression deformation of strata. By comparing the calculated settlement to the monitoring data, the validity and accuracy of the MatDEM model were verified. The area prone to earth fissures was predicted based on the analysis of the particle connections and horizontal displacement. The formation mechanism of the buried hill-controlled earth fissures was also explained. Thus, MatDEM is a good numerical simulation method for studying discontinuous problems, such as rock and soil cracking, and can be a new tool with which to study earth fissures.

Key words: Discrete element method (DEM); MatDEM; Buried hill; Earth fissure; Prone area
https://doi.org/10.1631/jzus.A1900292 **CLC number:** P642.26

1 Introduction

An earth fissure is a type of geological disaster associated with rapid economic growth and has caused considerable financial losses in past decades (Wang et al., 2016). The evolution of earth fissures has various causes including seismic activity, active faults, mining, and groundwater extraction (Peng et al., 2018; Howard and Zhou, 2019). In southern Jiangsu, China, the earth fissures were mainly caused by excessive groundwater extraction (Zhang et al., 2016; Zhang Y et al., 2018). In-depth research was conducted on the causes and characteristics of earth fissures that develop in this area via on-site exploration and numerical simulation (Wang et al., 2016; Mohseni et al., 2017). Based on the analysis of the engineering geological conditions and investigation of earth fissures in the Su-Xi-Chang area, China, Wu et al. (2010) found that uneven settlement caused by the excessive drainage of groundwater was the leading factor causing earth fissures. Before this, the same conclusion was drawn based on an analysis of the geodetic data of earth fissures in Hetang and Changjing in the Su-Xi-Chang area (Wang et al., 2009). Gong et al. (2018) conducted a laboratory

‡ Corresponding author
* Project supported by the National Natural Science Foundation of China (Nos. 41572271 and 41772327), the Open Project of Key Laboratory of Earth Fissures Geological Disaster of the Ministry of Land and Resources (No. JSDDY-HJ-D-2018-021), the Natural Science Foundation of Jiangsu Province (No. BK20161239), and the Open Fund of National Laboratory for Marine Science and Technology (Qingdao) (No. QNLM2016ORP0110), China
ORCID: Yang LIU, https://orcid.org/0000-0001-7147-7584

model test on the process of the evolution of earth fissures caused by water extraction.

Numerical simulation is also an important method used to research earth fissures. Ye et al. (2018) proposed a model suitable for use with the finite element method (FEM) and verified the evolution of earth fissures by comparing the results of this method to site investigations at Guangming village in Wuxi, China. Budhu (2011) interpreted the causes of earth fissures using the Mohr–Coulomb criterion. Panda et al. (2015) used a 2D FEM to perform the coupling modeling of seepage, stress, strain, etc. The simulation results were applied to predict earth fissures in the Phoenix flood control facilities. Burbey (2010) investigated a region prone to earth fissures by studying the changes in tensile and shear stresses caused by the excessive exploitation of groundwater near an existing fault.

However, FEM is not an ideal method for simulating discontinuous geological bodies such as earth fissures and cracks (Adiyaman, 2012; Yuan and Zhong, 2017). The main advantage of the discrete element method (DEM) over FEM is that, for the former, there is no need to mesh the model (Li et al., 2017; Zhang Y et al., 2018; Zhang ZH et al., 2018). DEM allows large deformations and fractures based on the movements of particles. Therefore, it is more suitable for simulating discontinuous problems. Therefore, it is advisable to apply DEMs to analyze the cause of and predict areas prone to earth fissures.

2 Principle of MatDEM

Cundall and Strack (1979) first proposed the idea of the DEM to study the relationship between particles. The dynamic motion process of particle stacks can be simulated using the time step method. The motion between the particles can be approximated as linear in a short time step. By calculating the force, displacement, velocity, and acceleration of the particles in this time step, a numerical simulation of the moving process of all granules is completed using iterative calculations (Mora and Place, 1994; Li et al., 2017).

Based on the above basic principles of discrete elements, researchers at Nanjing University independently developed the large-scale distinct element numerical simulation code MatDEM^{3D}. This code uses a graphics processing unit (GPU) matrix operation that is several times faster than central processing unit (CPU) based commercial DEM codes.

This study established a DEM model using MatDEM. The model consists of a series of particles that conform to Newtonian equations of motion. A breakable elastic spring connects the particles, and this spring acts only on the contact points between adjacent particles (Liu et al., 2013).

The interaction between particles through a normal spring force (F_n) is expressed as follows:

$$F_n=K_n\cdot X_n, \tag{1}$$

where K_n is the normal stiffness, and X_n is the relative normal displacement (Fig. 1b).

When the particles are connected, initially, there is a spring force between them (Eq. (1)). The normal spring force is positive. When the relative normal displacement between two particles X_n exceeds the breaking displacement X_b, the connection between the particles breaks and tension disappears. The maximum normal force between particles under intact bond conditions is expressed as

$$F_{nmax}=K_n\cdot X_b. \tag{2}$$

If the connection breaks in the opening mode and the tensile force between the particles ceases to exist, the normal spring force is zero. However, the repulsive force still exists between two particles when they return to a state of compressive contact (Eq. (3)). The normal spring force here is negative (Liu et al., 2015).

$$F_n=K_n\cdot X_n, \quad X_n<0. \tag{3}$$

Fig. 1c shows two particles joined in the tangential direction using a rupturable spring to simulate the shear deformation and the shear forces. The shear force (F_s) is expressed as follows:

$$F_s=K_s\cdot X_s, \tag{4}$$

where K_s is the shear stiffness and X_s is the tangential relative displacement between two particles. In numerical simulations, shear force is accumulated by calculating each time step (Cundall and Strack, 1979).

For a complete connection, the maximum shear force of the intact bond F_{smax} is determined using the Coulomb friction:

$$F_{smax}=F_{s0}-\mu_p F_n, \tag{5}$$

where F_{s0} is the inter-particle shear resistance, μ_p is the inter-particle coefficient of friction, and F_n is the normal force (compressive force is negative). When the external force exceeds F_{smax}, the intact connection between two particles breaks. The magnitude of the shear force (F_s) is limited to less than or equal to F_{smax}. The shear force of the broken bond $F_{smax'}$ is expressed as follows:

$$F_{smax'}=-\mu_p F_n. \tag{6}$$

When the inter-particle shear force exceeds the maximum shear force $F_{smax'}$, the inter-particle connection breaks and the particles undergo relative displacement. The sliding friction between particles is $F_{smax'}$.

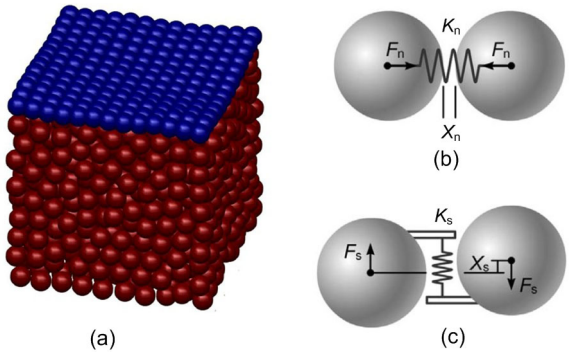

Fig. 1 Schematic diagram of DEM

(a) A close-packed DEM of breakable elastic spring bonds; (b) Two elements bonded by a breakable elastic spring, which interact through a spring force; (c) Two elements bonded by a spring along the tangential direction to simulate the shear force (F_s)

3 Model and parameters

3.1 Geological prototype

The Shitangwan earth fissure in Wuxi, in the Su-Xi-Chang area, was selected as the research object; it is one of the three major earth fissure regions in China. The depth of the central crack is approximately 500 mm (Wang et al., 2009). The Geological Survey of Jiangsu Province drilled five vertical holes perpendicular to the main crack. Fig. 2 shows stratigraphic cross section based on drilling data and field investigation. The strike of the buried hill is north-east-east, and the buried depth of the ridge is approximately 50 m. The spacing between boreholes Wf1 and Wf2 is about 460 m. A main confined aquifer exists in the north side of the buried hill, and the buried depth is approximately 90–120 m. The stratum above the confined aquifer is mainly composed of silty clay. A phenomenon of silty clay and silt interbed can be found at a depth of 20–40 m. There are several sand lenses of thickness less than 5 m under 40 m below the ground surface (Wang et al., 2017). According to the field survey, there is an earth fissure zone between S02 and S03 that is approximately 60 m wide; two main fissures are developed there.

3.2 2D DEM model with particle accumulation

To simplify the modeling, sand lenses between depths of 40 m and 60 m were omitted. At the same time, the established model box in the modeling process was made slightly larger than the study area to minimize the influence of the boundary effects on the numerical simulation. The model box is 800 m× 200 m, and is composed of 19070 balls with an average diameter of 1.5 m.

A close-packed DEM model was initially obtained by the accumulation of particles in the model box due to gravity. According to the data on the boreholes, an elevation table indicating the interfaces of the strata was constructed, based on which a custom cutting function was built. A 2D layered DEM model was established for simulation by importing the cutting function into the initial model. Different parameters were then set for each stratum.

3.3 Parameters and model balance

3.3.1 Macroscopic parameter for MatDEM

In MatDEM, the macroscopic parameters mainly include density (ρ), Young's modulus (E), Poisson's ratio (υ), tensile strength (T_u), compressive strength (C_u), and internal friction coefficient (μ_p). These physical and mechanical parameters are usually determined by conducting specific experiments or back analysis based on field monitoring. The macroscopic parameters are listed in Table 1.

3.3.2 Inter-particle parameter for MatDEM

The relationship between particles in MatDEM mainly depends on six inter-particle parameters: normal and shear stiffness, breaking displacement, shear resistance, coefficient of friction, and unit mass. Liu et al. (2013) verified the conversion formula between the macro- and microscopic parameters through experiments. Considering normal stiffness as an example, Eq. (7) shows the relationship between the normal stiffness, Young's modulus, and Poisson's ratio, which is suitable for the tightly regular stacking model of equal spherical elements.

$$K_{\mathrm{n}}=\frac{\sqrt{2}Ed}{4(1-2\upsilon)}, \tag{7}$$

where d is the element diameter.

The inter-particle parameters of different layers in the MatDEM model were set according to Table 2. After that, gravity was applied to the whole model until a balanced state was achieved again.

DEM also needs to simulate the energy dissipation process in the real world to avoid the accumulation of mechanical energy in the model. The damping in DEM was usually used to indicate the dissipation of mechanical energy. Therefore, the balanced state of the entire model can be determined according to the damping force between particles. Fig. 3 shows the damping force in the Z-direction of the model after achieving a balanced state. It can be seen that the force between the model particles is almost zero. Overall, the model is in equilibrium.

$$F_{\mathrm{v}}=-\eta\cdot x, \tag{8}$$

where F_{v} is the global damping representing a simple definition of the damping force, η represents the damping coefficient, and x represents the velocity. The optimal damping of the model can be obtained using the empirical formula (Liu et al., 2017).

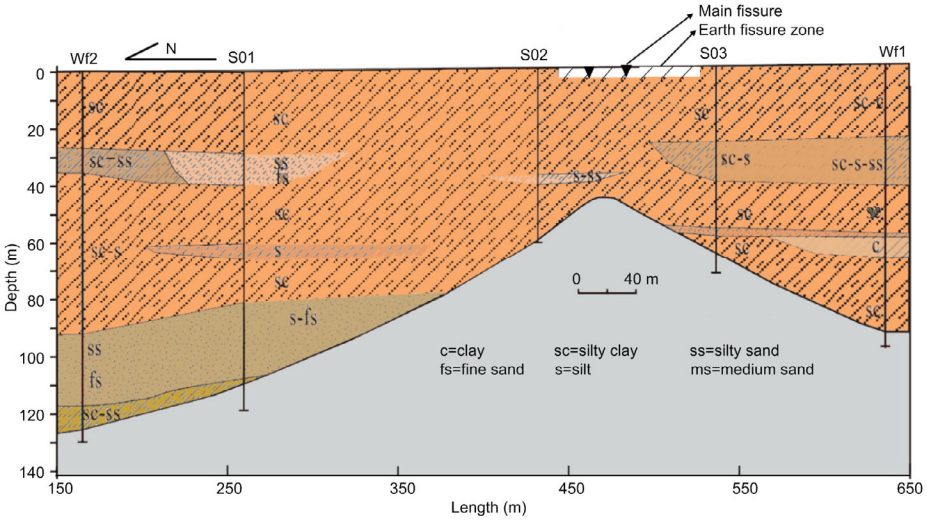

Fig. 2 Stratigraphic cross section

Table 1 Macroscopic parameters of clay and sand

Parameter	Value	
	Clay	Sand
Density, ρ (g/cm^3)	2.05	2.00
Young's modulus, E (Pa)	2.00×10^7	1.60×10^8
Poisson's ratio, υ	0.16	0.16
Tensile strength, T_{u} (Pa)	2.04×10^3	1.00×10^4
Compressive strength, C_{u} (Pa)	2.70×10^4	1.00×10^5
Coefficient of friction, μ_{p}	0.8	1.0

Table 2 Inter-particle parameters of clay and sand for MatDEM

Parameter	Value	
	Clay	Sand
Normal stiffness, K_{n} (Pa)	7.7368×10^7	2.1015×10^8
Shear stiffness, K_{s} (Pa)	2.4692×10^7	3.6233×10^7
Fracture displacement, X_{b} (m)	1.0348×10^{-4}	2.0485×10^{-5}
Initial shear force, F_{s0} (N)	3.5869×10^4	1.9365×10^4
Coefficient of friction, μ_{p}	0.2547	0.1453
Unit mass, m (kg)	5.9070×10^3	5.5378×10^3

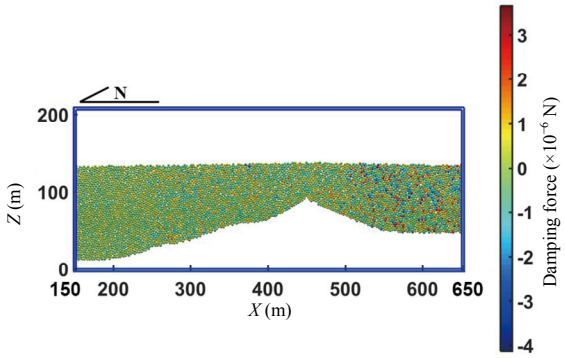

Fig. 3 Damping force in *Z*-direction

3.4 Simplified algorithm for fluid-structure interaction

The lattice Boltzmann method was used for the fluid-structure interaction problem in DEM (Han and Cundall, 2013; Redaelli et al., 2017). A few commercial software programs did not run efficiently because there was a large amount of calculation involved (Scaringi et al., 2018). To simulate large geological bodies, too few particles can make the simulation results deviate significantly from the actual situation. Hence, to simplify the problem of excessive calculations of fluid-structure interaction during simulations of earth fissures, a quasi-fluid structure interaction method was adopted (Dai et al., 2017; Scaringi et al., 2018; Demir et al., 2019).

The vertical force of particles F_v below the water level can be expressed as

$$F_v=F_f+G+F_{n,v}+F_{s,v}, \tag{9}$$

where F_f is the buoyancy of the particle, which depends on the volume of the particle, G is the gravity of the particle, $F_{n,v}$ is the vertical vector of the particle normal force, and $F_{s,v}$ is the vertical vector of the particle shear force. When the water level was lowered, the upward buoyancy F_f disappeared for all the particles above the water level. The calculation was conducted until a balanced state was achieved. The strata deformation due to the effect of water level reduction was obtained.

4 Simulation results and analysis

4.1 Model verification

According to the monitoring data from the Geological Survey of Jiangsu Province, China, the water table dropped 80 m before the groundwater extraction was completely banned in this area (Wang et al., 2010a), as shown in Fig. 4. To study the development process of earth fissures during the groundwater extraction, the water level was decreased by 10 m/step with the initial water level of 10 m below the ground.

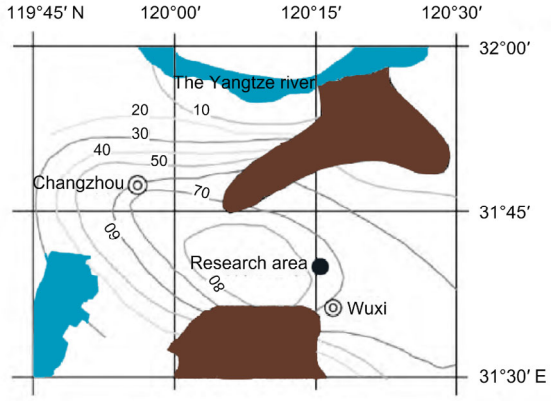

Fig. 4 Groundwater drawdown in Su-Xi-Chang area, China (unit: m)

A point at the location of 150 m (x=150 m, z=143 m) in the model (at the foot of the mountain rock) was selected as the reference point. The calculated settlements of the reference point indicating the lowering process of the water level are shown in Fig. 5. The average settlement of the study area was between 800 mm and 1000 mm since 1979. According to the geological survey, the groundwater drawdown reached 40 m in 1985 and 80 m in 2000 (Wang et al., 2010b). The calculated settlements were basically consistent with the monitoring data of the Su-Xi-Chang area, thereby verifying the reliability of the DEM model in this study.

4.2 Displacements in *Z*-direction

Considering the groundwater drawdown of 40 m as an example, Fig. 6a shows the *Z*-direction displacement. It can be seen that the displacement at the foot of both sides of the buried hill is more and that at the ridge is less. The maximum *Z*-direction displacement was 0.63 m. Fig. 6b shows the

displacement in the *Z*-direction when the groundwater drawdown was 80 m, and the distribution of the displacement is similar to that of the drawdown at 40 m. However, the maximum displacement of the drawdown at 80 m was 0.94 m.

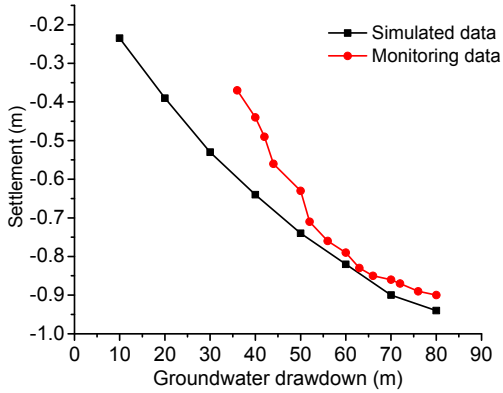

Fig. 5 Comparison between simulated and monitored settlements

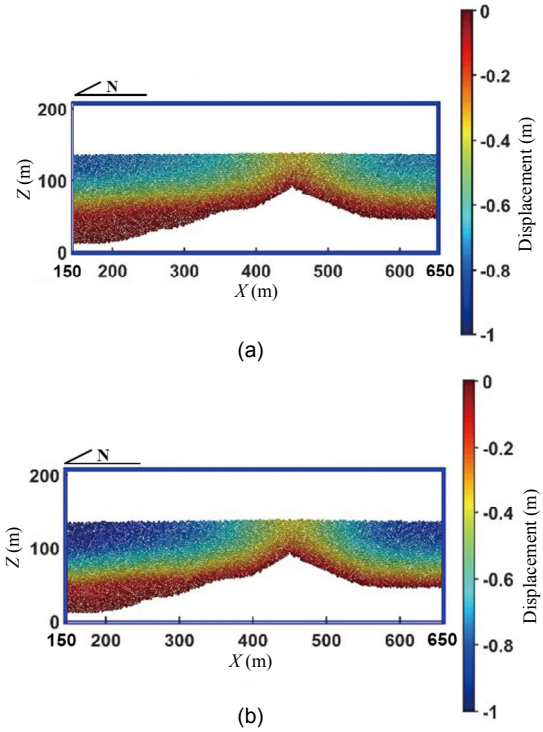

Fig. 6 Displacement in the *Z*-direction due to groundwater drawdown at 40 m (a) and at 80 m (b)

The ground settlements on both sides of the ridge were recorded at a distance of every 50 m. As the differential settlement above the ridge is larger, the smaller distance between the recorded points was adopted. The recorded settlements were calculated based on the average displacement of particles in a certain area.

Fig. 7 shows the settlements of the ground surface. With the increase in the water level drawdown, the amount of sedimentation decreases gradually along the horizontal distance. By comparing the ground settlements during the lowering process of the water level, the total settlement on the north side of the ridge was observed to be slightly larger than those on the south side because the deposit on the north side of the ridge was thicker. The settlement at the ridge is the smallest, as shown in Fig. 7, at the range of (450±10) m along the horizontal distance because of the thin deposit. The difference between the ridge and foot of the buried hill increased during the water level drawdown. Therefore, the sediments near the ground surface were bent because of the water level drawdown.

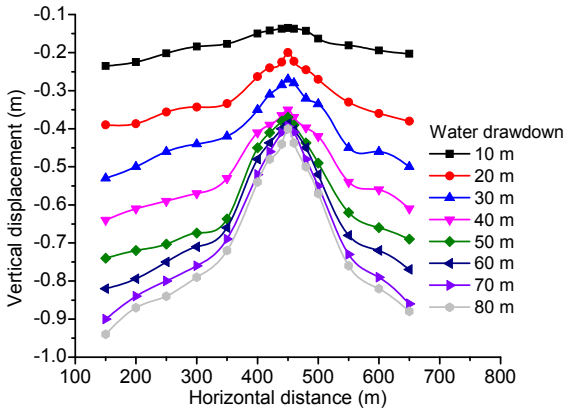

Fig. 7 Different water level depths

4.3 Unit connection of DEM model

DEM has the most advantages, compared to FEM and finite difference method (FDM), in terms of simulating discontinuities; thus, it can be regarded as a model consisting of abundant particles connected by a "spring." This "spring" can be broken when the connection between the particles exceeds the fracture displacement (Neveu et al., 2016; Liu et al., 2017). It is easy to visualize the cracking process and prone area of earth fissures. Fig. 8a shows the overall unit connection of the DEM model; Fig. 8b is a magnified

view of the unit connection. It can be seen that there is an apparent regional breakage of the unit connection above the ridge, which indicates that inter-particle displacement was larger than the fracture. In the model, there were dislocations and large displacements between particles, which shows that the geological body was prone to disconnection and cracks. Therefore, earth fissures are more likely to occur in the area where the region of unit disconnection is observed.

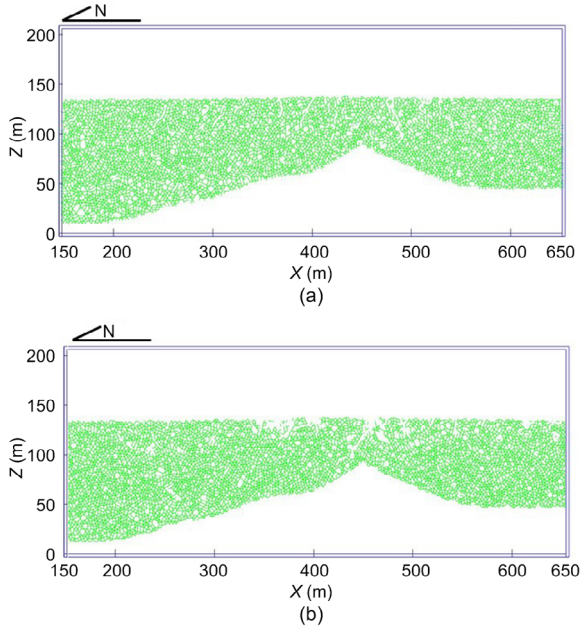

Fig. 8 Comparison of unit connection before and after water extraction
(a) Before simulation; (b) Simulation results

4.4 *X*-direction displacement

The studies of earth fissures caused by excessive water extraction indicate that horizontal displacement of formations may play an important role in the development process (Rothenburg et al., 1995; Yoo and Perrings, 2017). Figs. 9a and 9b show the displacement in the *X*-direction at 40 m and 80 m, respectively. Apparently, the directions of the displacement on both sides of the buried hill ridge are different. The displacement of particles is negative on the north side, and positive on the south side because the sediments near the ground surface are in a bending state during the water level drawdown. Therefore, the breakage of the unit connection above the ridge was mainly controlled by the *X*-direction displacement.

Fig. 10 shows the location and strike direction of earth fissures determined by the field investigation and the positional relationship with the borehole. The earth fissure zone was located between boreholes S02 and S03, which is consistent with simulation results from MatDEM.

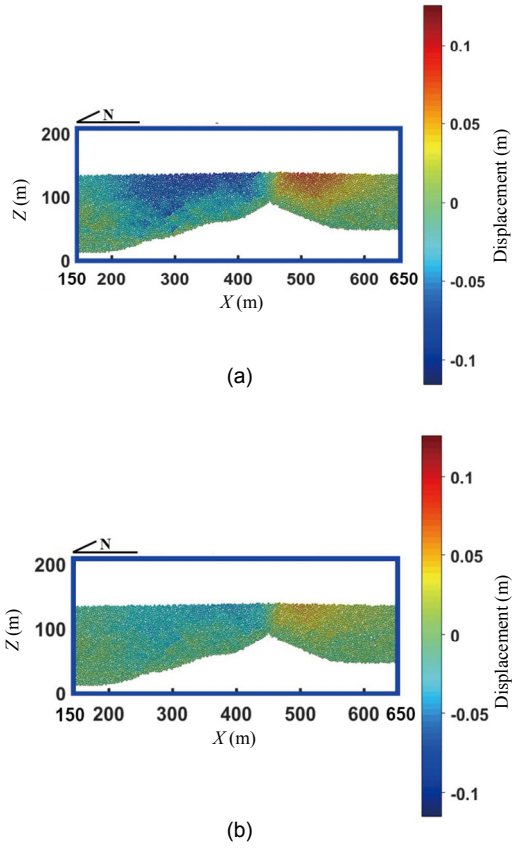

Fig. 9 Displacement in the *X*-direction due to groundwater drawdown at 40 m (a) and at 80 m (b)

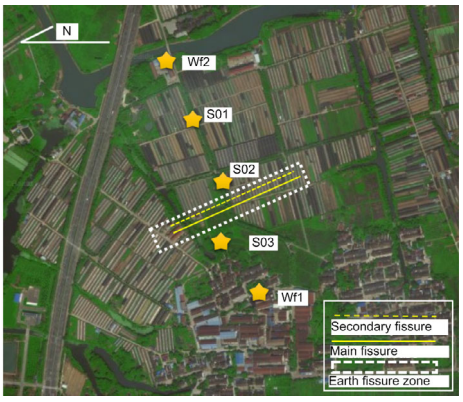

Fig. 10 Location of earth fissures according to the geological survey

5 Conclusions

MatDEM, a code of DEM, was used to predict the prone area of earth fissures in the Su-Xi-Chang area, China. The simulation results were compared to the on-site settlement monitoring data and the geological survey. The feasibility of the DEM model in the numerical simulation of earth fissures is verified. Main conclusions are given as follows:

1. The *Z*-direction displacement above the ridge was smaller than that on both sides of the buried hill, resulting in a bending effect on the soil near the ground surface. It can be inferred that bending due to an uneven settlement during the groundwater drawdown is the main mechanism of the buried hill-controlled earth fissures. The mechanism can also be verified by the *X*-direction displacement near the ground surface, which is opposite around the ridge of buried hill, and the breakage of the unit connections of particles above the ridge. Therefore, the displacement and unit connections of particles can be considered indicators for the development of earth fissures.

2. MatDEM is a reliable and intuitive numerical simulation method to solve the discontinuous problems, such as earth fissures, that is simplified by considering the interaction between particles. The method can be used to predict the prone area of buried hill-controlled earth fissures and study the evolution process of earth fissures.

Contributors

Yang LIU simulated and wrote the manuscript. Dan ZHANG provided the idea. Guang-ya WANG and Yan ZHANG provided geological survey data. Chun LIU helped solve software problems.

Conflict of interest

Yang LIU, Dan ZHANG, Guang-ya WANG, Chun LIU, and Yan ZHANG declare that they have no conflict of interest.

References

Adiyaman IB, 2012. Land Subsidence and Earth Fissures Due to Groundwater Pumping. PhD Thesis, University of Arizona, Arizona, USA.

Budhu M, 2011. Earth fissure formation from the mechanics of groundwater pumping. *International Journal of Geomechanics*, 11(1):1-11. https://doi.org/10.1061/(ASCE)GM.1943-5622.0000060

Burbey TJ, 2010. Mechanisms for earth fissure formation in heavily pumped basins. *In*: Land Subsidence, Associated Hazards and the Role of Natural Resources Development. IAHS-AISH Publication, Querétaro, Mexico.

Cundall PA, Strack ODL, 1979. A discrete numerical model for granular assemblies. *Géotechnique*, 29(1):47-65. https://doi.org/10.1680/geot.1979.29.1.47

Dai ZL, Huang Y, Cheng HL, et al., 2017. SPH model for fluid–structure interaction and its application to debris flow impact estimation. *Landslides*, 14(3):917-928. https://doi.org/10.1007/s10346-016-0777-4

Demir A, Dincer AE, Bozkus Z, et al., 2019. Numerical and experimental investigation of damping in a dam-break problem with fluid-structure interaction. *Journal of Zhejiang University-SCIENCE A (Applied Physics & Engineering)*, 20(4):258-271. https://doi.org/10.1631/jzus.A1800520

Gong XL, Gu CS, Lu Y, et al., 2018. Model test for evolution of ground fissures due to extraction of groundwater. *Journal of Engineering Geology*, 26(4):951-958 (in Chinese). https://doi.org/10.13544/j.cnki.jeg.2017-342

Han YH, Cundall PA, 2013. LBM–DEM modeling of fluid–solid interaction in porous media. *International Journal for Numerical and Analytical Methods in Geomechanics*, 37(10):1391-1407. https://doi.org/10.1002/nag.2096

Howard KWF, Zhou WF, 2019. Overview of ground fissure research in China. *Environmental Earth Sciences*, 78(3):97. https://doi.org/10.1007/s12665-019-8114-6

Li WT, Yang N, Li TC, et al., 2017. A new approach to simulate the supporting arch in a tunnel based on improvement of the beam element in FLAC^{3D}. *Journal of Zhejiang University-SCIENCE A (Applied Physics & Engineering)*, 18(3):179-193. https://doi.org/10.1631/jzus.A1600508

Liu C, Pollard DD, Shi B, 2013. Analytical solutions and numerical tests of elastic and failure behaviors of close-packed lattice for brittle rocks and crystals. *Journal of Geophysical Research: Solid Earth*, 118(1):71-82. https://doi.org/10.1029/2012JB009615

Liu C, Pollard DD, Gu K, et al., 2015. Mechanism of formation of wiggly compaction bands in porous sandstone: 2. Numerical simulation using discrete element method. *Journal of Geophysical Research: Solid Earth*, 120(12):8153-8168. https://doi.org/10.1002/2015JB012374

Liu C, Xu Q, Shi B, et al., 2017. Mechanical properties and energy conversion of 3D close-packed lattice model for brittle rocks. *Computers & Geosciences*, 103:12-20.

https://doi.org/10.1016/j.cageo.2017.03.003

Mora P, Place D, 1994. Simulation of the frictional stick-slip instability. *Pure and Applied Geophysics*, 143(1-3):61-87. https://doi.org/10.1007/BF00874324

Mohseni N, Sepehr A, Hosseinzadeh SR, et al., 2017. Variations in spatial patterns of soil–vegetation properties over subsidence-related ground fissures at an arid ecotone in northeastern Iran. *Environmental Earth Sciences*, 76(6): 234. https://doi.org/10.1007/s12665-017-6559-z

Neveu A, Artoni R, Richard P, et al., 2016. Fracture of granular materials composed of arbitrary grain shapes: a new cohesive interaction model. *Journal of the Mechanics and Physics of Solids*, 95:308-319. https://doi.org/10.1016/j.jmps.2016.06.008

Panda BB, Rucker ML, Fergason KC, 2015. Modeling of earth fissures caused by land subsidence due to groundwater withdrawal. *Proceedings of the International Association of Hydrological Sciences*, 372:69-72. https://doi.org/10.5194/piahs-372-69-2015

Peng JB, Meng LC, Lu QZ, et al., 2018. Development characteristics and mechanisms of the Taigu–Qixian earth fissure group in the Taiyuan basin, China. *Environmental Earth Sciences*, 77(11):407. https://doi.org/10.1007/s12665-018-7570-8

Redaelli I, Ceccato F, di Prisco C, et al., 2017. Solid-fluid transition in granular flows: MPM simulations with a new constitutive approach. *Procedia Engineering*, 175:80-85. https://doi.org/10.1016/j.proeng.2017.01.028

Rothenburg L, Obah A, El Baruni S, 1995. Horizontal ground movements due to water abstraction and formation of earth fissures. *International Association of Hydrological Sciences, Publication*, 234:239-249.

Scaringi G, Fan XM, Xu Q, et al., 2018. Some considerations on the use of numerical methods to simulate past landslides and possible new failures: the case of the recent Xinmo landslide (Sichuan, China). *Landslides*, 15(7): 1359-1375. https://doi.org/10.1007/s10346-018-0953-9

Wang GY, You GG, Shi B, et al., 2009. Earth fissures triggered by groundwater withdrawal and coupled by geological structures in Jiangsu Province, China. *Environmental Geology*, 57(5):1047-1054. https://doi.org/10.1007/s00254-008-1390-1

Wang GY, You GG, Shi B, et al., 2010a. Earth fissures in Jiangsu Province, China and geological investigation of Hetang earth fissure. *Environmental Earth Sciences*, 60(1):35-43. https://doi.org/10.1007/s12665-009-0167-5

Wang GY, You GG, Shi B, et al., 2010b. Large differential land subsidence and earth fissures in Jiangyin, China. *Environmental Earth Sciences*, 61(5):1085-1093. https://doi.org/10.1007/s12665-009-0430-9

Wang GY, You GG, Zhu JQ, et al., 2016. Investigations of Changjing earth fissures, Jiangyin, Jiangsu, China. *Environmental Earth Sciences*, 75(6):502. https://doi.org/10.1007/s12665-015-5163-3

Wang GY, Zhu JQ, You GG, et al., 2017. Land rebound after banning deep groundwater extraction in Changzhou, China. *Engineering Geology*, 229:13-20. https://doi.org/10.1016/j.enggeo.2017.09.006

Wu JC, Shi XQ, Ye SJ, et al., 2010. Numerical simulation of viscoelastoplastic land subsidence due to groundwater overdrafting in Shanghai, China. *Journal of Hydrologic Engineering*, 15(3):223-236. https://doi.org/10.1061/(ASCE)HE.1943-5584.0000172

Ye SJ, Franceschini A, Zhang Y, et al., 2018. A novel approach to model earth fissure caused by extensive aquifer exploitation and its application to the Wuxi case, China. *Water Resources Research*, 54(3):2249-2269. https://doi.org/10.1002/2017WR021872

Yoo J, Perrings C, 2017. An externality of groundwater depletion: land subsidence and residential property prices in Phoenix, Arizona. *Journal of Environmental Economics and Policy*, 6(2):121-133. https://doi.org/10.1080/21606544.2016.1226198

Yuan S, Zhong HZ, 2017. Finite deformation elasto-plastic consolidation analysis of soft clay by the weak form quadrature element method. *Journal of Zhejiang University-SCIENCE A (Applied Physics & Engineering)*, 18(2):942-957. https://doi.org/10.1631/jzus.A1600671

Zhang Y, Wang ZC, Xue YQ, et al., 2016. Mechanisms for earth fissure formation due to groundwater extraction in the Su-Xi-Chang area, China. *Bulletin of Engineering Geology and the Environment*, 75(2):745-760. https://doi.org/10.1007/s10064-015-0775-0

Zhang Y, Yu J, Gong XL, et al., 2018. Pumping-induced stress and strain in aquifer systems in Wuxi, China. *Hydrogeology Journal*, 26(3):771-787. https://doi.org/10.1007/s10040-017-1697-7

Zhang ZH, Zhang XD, Tang Y, et al., 2018. Discrete element analysis of a cross-river tunnel under random vibration levels induced by trains operating during the flood season. *Journal of Zhejiang University-SCIENCE A (Applied Physics & Engineering)*, 19(5):346-366. https://doi.org/10.1631/jzus.A1700002

中文概要

题　目：基于离散元法的基岩潜山型地裂缝易发区预测

目　的：采用离散元法揭示抽水引起的基岩潜山型地裂缝的发育过程，实现对地裂缝易发区的准确预测，为地裂缝灾害的早期预测和防治提供依据。

创新点： 1. 提出采用离散元法模拟抽水引起的地裂缝问题。2. 提出依据颗粒连接和水平位移等预测地裂缝的易发区。

方　法： 1. 建立一个紧密堆积的二维模型。2. 通过地调得到的高程切割模型，构建二维地层模型。3. 对不同地层进行材料参数赋值，随后施加重力，并对模型进行平衡。4. 模型达到平衡后，采用简化的流固耦合计算方法以及通过调整单元颗粒的浮力来模拟降水过程。5. 通过每次运算降低 10 m 地下水位的循环算法模拟在地下水逐渐降低过程中的地裂缝发展。6. 通过与现场地调数据进行对比，验证离散元法在地裂缝模拟中的可靠性。

结　论： 1. 随着地下水位的下降，由于不均匀沉降而产生的土体弯曲作用是控制地裂缝发育的主要机制。2. MatDEM 是一种更可靠、直观的数值模拟方法，可以用于不连续地质体（如基岩潜山型）地裂缝的易发区预测，以及地裂缝的演化过程研究。

关键词： 离散元法；MatDEM；基岩潜山型地裂缝；易发区